Desalination and Water Treatment
www.deswater.com
doi:10.5004/dwt.2017.21474

93 (2017) 109–119
October

Sorption of humic acid to layered double hydroxides prepared through ion thermal method

Pei Zhong, Kefeng Ping, Xinhong Qiu*, Fengxi Chen*

School of Chemistry and Environmental Engineering, Wuhan Institute of Technology, Wuhan 430073, China,
email: witzhongpei@163.com (P. Zhong), 576435836@qq.com (K. Ping), qxinhong@gmail.com (X. Qiu), fxchen@wit.edu.cn (F. Chen)

Received 26 April 2017; Accepted 21 September 2017

ABSTRACT

Ultrathin layered double hydroxides (LDHs) with small particle size were synthesized using a deep eutectic solvent (I-LDH) and were applied for humic acid removal. The characteristics of I-LDH and its calcinated product (I-CLDH) were analyzed via SEM, TEM, FTIR, XRD, AFM, and BET. The morphologies of I-LDH and I-CLDH were similar. The mean particle size was around 10–40 nm and formed a monolayer of around 0.7 nm. The removal of humic acid followed pseudo-first-order kinetics, and the sorption capacity was improved via calcination. Based on the Langmuir sorption isotherm, the sorption capacity of I-CLDH reached 43.11 mg/g. The results of measuring the samples after sorption (via XRD, SEM, and FTIR) suggested that the sorption of humic acid onto LDHs occurred by intercalation and surface sorption. In addition, the pH value had a slight effect on sorption performance, and the coexisting anions in the environment (especially carbonates) had an inhibitory effect on the sorption.

Keywords: Humic acid; Ionothermal synthesis; LDH; Sorption

1. Introduction

Humic acid is heterogeneous and contains different functional groups and different levels of molecular weight polymers, with high molecular weight and high stability [1]. It is typically present in rivers and lakes and thus it may pose a problem for drinking water production since it can impart a yellow-brownish color and cause an unpleasant taste of the water [2]. HA can potentially form carcinogenic disinfection byproducts (DPBs) (e.g., trihalomethanes and haloacetic acids) during the chlorination of drinking water, which have fouling potential of membranes and ion-exchange resins [3,4]. Furthermore, concern has been growing over the adverse effects of humic acid on living organisms due to its persistence and poor biodegradability [2,5,6]. However, humic acid was found to influence the migration of radionuclides and trace metals [7–12]. For example, Singh et al. reported in 2009 that the present of humic acid has a negligible effect on sorption of 137Cs, 90Sr, 154Eu, and 141Ce via magnetite [8]. In 2011, Singh et al. reported that the sorption of trace metal ions on synthesized sodium aluminosilicate was also influenced by humic acid [9]. Furthermore, the authors suggested that the short-chain carboxylic acids showed stronger aqueous complexation properties towards the uranyl ions in solution than sorbed uranyl onto rutile [11]. Therefore, humic acid remains one of the main substances that are measured and the development of effective methods for humic acid removal is essential.

Traditional methods for humic acid removal during drinking water production are membrane separation and chemical coagulation [2]. Membranes can be fouled by humic acid and thus limit its application in this field. Coagulation via alum has been widely used, which results in high operational costs and generates high volumes of additional sludge [13]. Compared to this, sorption is characterized by simple operation and cost effectivity, thus offering high practical value for water treatment methods [14]. The most commonly used adsorbents for environmental remediation are activated carbon, clay materials, and modified oxide/hydroxide nanomaterials

*Corresponding authors.

[15,16]. Among all these adsorbents, LDH (an anion exchange clay material) can be considered as a potentially costly and less efficient adsorbent [17]. Furthermore, other materials have similar shortcomings such as high prices, high operating costs, and poor disposal of sludge [2]. This is due to the presence of anionic layers with high ion exchange properties in their structure. The general formula of LDHs is $^{X+}(A^{n-})_{x/n}\cdot H_2O$, where M^{2+} and M^{3+} are divalent and trivalent cations, respectively, X is $M^{3+}/(M^{2+} + M^{3+})$, and *A* is the interlayer anion with valence *n*. A wide variety of M^{2+}, M^{3+}, X, and A^{n-} are endowed to a large class of iso-structural materials with various physical and chemical properties [18,19]. LDHs can uptake anion species from solutions via three mechanisms: surface sorption, interlayer anion exchange, and reconstruction of a calcined LDH precursor using the "memory effect" [20]. In 2015, Fang et al. calcined LDH was used to remove metallic element Ni in both presence and absence of humic acid (HA) and FA. The HA or FA bound on the surface of the rehydrated LDH can induce an additional Ni(II)-HA or -FA complexation; thus, leading to the enhancement of Ni removal [21]. Peligro et al. studied heavy metal removal from a simulated mining wastewater that was sorpted by a carbonate-intercalated Mg-Al LDH (LDH-CO_3^{2-}) or in situ precipitation of LDH [22]. A MoS_2^{4-} ion was intercalated into MgAl-NO_{3-} LDH by Ma et al. to produce a single-phase material, which demonstrated highly selective binding and extremely efficient removal of heavy metal ions [23].

A new synthesized method for directly preparing the LDHs with small particles sizes is considered as a more convenient and straightforward approach [24]. For example, Fang et al. developed an upscale facile method and successfully prepared a layered Fe-III nanosheets material. This material showed strong adsorption selectivity towards phosphate even in the presence of high concentrations of background ions [25]. Similar to traditional ionic liquids, deep eutectic solvent (DES) can also be used as an ionic reaction medium and provide a unique ionic environment for reactions. Thus, different materials with nanometer functions can be prepared in DES [26–28]. In particular, ionic liquid can not only control the growth of pellet sizes, but also significantly improve physicochemical properties of material surfaces and improve their stability. Recently, prepared Mg-Al LDHs comprising a mixture of choline chloride and urea at a 1:2 molar ratio (in short ChCl:2urea) has been developed by our group via ionothermal in a DES. The resulting product showed superior performance in the removal of borate compared the LDHs prepared via the urea method [19]. However, in contrast to borate, humic acid is an organic substance. The sorption behavior of humic acid by LDHs and its calcinated products should therefore be different from that of borate.

Therefore, considering the dangers of humic acid and expanding the applicable range of ultrathin Mg-Al LDH, the aim of this study was to synthesize Mg-Al-LDHs in a DES of choline chloride:urea (2:1). Samples were carefully characterized and applied in the removal of humic acid. Several factors, such as pH and co-existing anions that may affect the sorption performance were studied and the underlying mechanism was discussed.

2. Experimental

2.1. Chemicals

Magnesium nitrate hexahydrate, ($Mg(NO_3)_2\cdot 6H_2O$), aluminum nitrate nonahydrate ($Al(NO_3)_3\cdot 9H_2O$), urea (CH_4N_2O), choline chloride ($C_5H_{14}ClNO$), sodium hydroxide (NaOH), and potassium hydroxide (KOH) were obtained from Sinopharm Chemical Reagent Co. Ltd. All reagents were special grade and used as received, without purification. Humic acid (HA) used in this work is sodium humate and was also obtained from Aladdin Chemical Reagent Co. Ltd, as an analytical reagent.

2.2. Preparation of Mg-Al-LDH via ionothermal synthesis in a deep eutectic solvent

8.378 g of choline chloride and 7.07 g of urea were added into 50 mL of polytetrafluoroethylene (PTFE). The obtained solution was heated and stirred at 80°C to prepare the DES ion liquid. $Mg(NO_3)_2\cdot 6H_2O$ (1.54 g), and $Al(NO_3)_3\cdot 9H_2O$ (1.13 g) at a molar ratio of 2:1 were then added into the DES ion liquid and stirred for 5 min; then, 1.69 g of KOH were added and the mixed solution was stirred for 30 min, at a constant temperature of 100°C. Later, the reaction vessel was placed in a constant-temperature oven at 100°C for 48 h, after which the products were washed with deionized water and ethanol to neutralize them, and were dried in a vacuum drying oven at 50°C overnight. To improve the sorption performance in line with previous studies, the resulting product (I-LDH) was calcinated at 500°C (I-CLDH).

2.3. Characterization

The morphology of different samples was observed using a JSM-5510LV scanning electron microscope (SEM) (JEOL, Japan). The size of the synthesized nanoparticles was characterized using a JEM-2100 transmission electron microscope (TEM) (JEOL, Japan). After dispersion with an ultrasonic generator, the nanoparticle/ethanol mixture was deposited as a droplet on a carbon coated Cu grid. When the ethanol had completely evaporated, the sample was introduced into the vacuum chamber. The crystalline phase of the nanoparticles was measured via Cu K, radiation using a D8 Advance X-ray diffractometer (Bruker, Germany). The accelerating voltage and the applied current were 30 kV and 20 mA, respectively. Nitrogen adsorption-desorption measurements were performed on an MX-6 surface analyzer (BEL, Japan). FTIR measurements were conducted with a spectroscope Nicolet-6700 (Thermo Electron, USA). Thermogravimetric analysis (TG-DTA) was conducted from room temperature up to 800°C using a 2000SA differential thermal balance (Bruker, Germany) at a heating rate of 10°C/min.

2.4. Sorption experiments

A certain amount of humic acid sodium was measured by weight and dissolved to prepare the humic acid solution. Then, 0.100 g of product were added to 40 mL humic acid solutions, followed by shaking at 100 rpm at room

temperature using a shaking incubator. At certain time intervals, supernatants were filtered (0.20 μm) and the concentration of humic acid in the solution after adsorption was measured via UV-1800PC UV spectrophotometer (254 nm). The solid residue after sorption was collected and examined using SEM, XRD, and FTIR analysis. All sorption experiments were replicated thrice. The average values are shown in figures and tables.

3. Results and discussion

3.1. Characterization

The TG and DTA curves for I-LDH are shown in Fig. 1. Typical for LDHs, the weight loss essentially occurred in two steps [3]. The first stage started from 160°C and corresponded to 13.1% weight loss caused via evaporation of the surface adsorbed water and interlayer water of LDH. The second stage from 281°C to 596°C corresponded to a 25.5% weight loss caused via simultaneous elimination of intercalated CO_3^{2-}, strongly bound water, and the dehydroxylation of the brucite-like octahedral layers [18,29].

Fig. 2 shows the XRD patterns of I-LDH and I-CLDH, revealing that characteristic diffraction peaks of hydrotalcite appeared in the obtained material via ionothermal synthesis in a deep eutectic solvent, such as 003 peak around 11.7° and 006 around 23.5° [20]. The crystallinity of I-LDH prior to calcination was 267 Å and the d-space was 7.49 Å. After calcination, I-LDH was transformed into a MgO-like structure. According to a previous report, during the calcination of LDH, the aluminum atoms dissolved in the solid, which replaced the magnesium ion in the magnesium oxide to form a special structure of mixed oxides [30].

Fig. 3 shows the SEM image of I-LDH and I-CLDH. The morphologies of both samples were similar and small particles had aggregated. For more detailed observations, TEM was introduced for I-CLDH. In Fig. S1, I-CLDH appeared to have an irregular sheet structure. The size of it was about 10–40 nm. Furthermore, the thickness of I-CLDH was extremely thin. AFM shows (Fig. 4) that through

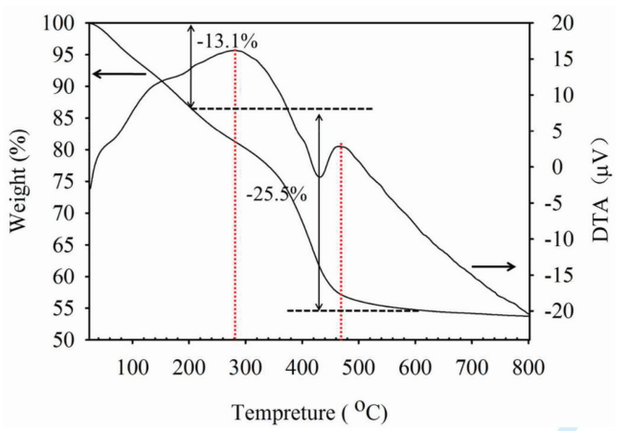

Fig. 1. TG and DTA of I-LDH.

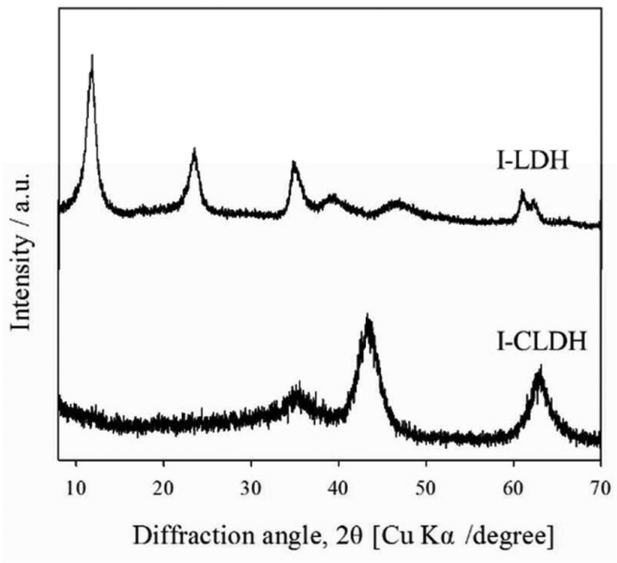

Fig. 2. XRD patterns of I-LDH and I-CLDH.

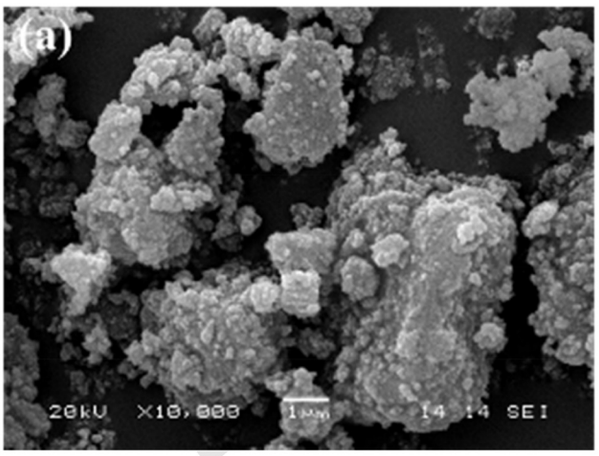

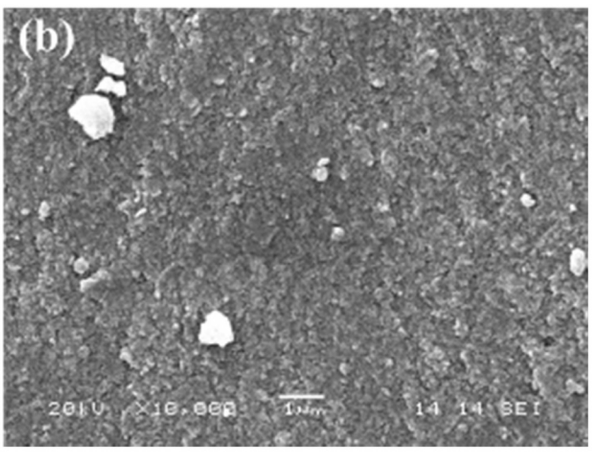

Fig. 3. SEM image of I-LDH and I-CLDH.

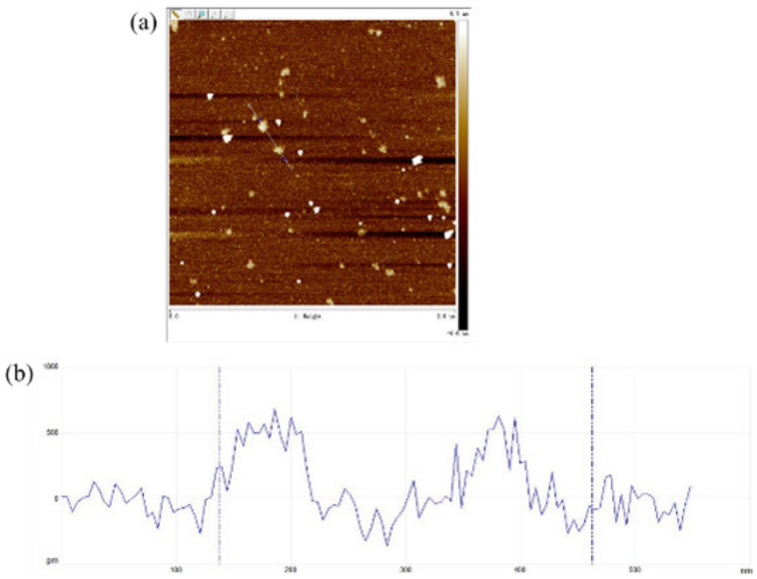

Fig. 4. AFM images of I-CLDH, (a) 1 × 1 μm area; (b) Cross-sectional analysis along the line in (a).

analyzing I-CLDH of different dispersions, its thickness was revealed to be around 0.7 nm. Moreover, the specific surface area of I-CLDH after calcination was 213.14 m^2/g due to smaller particle size.

Fig. S2 shows the FTIR characterizations of I-LDH and I-CLDH, respectively. Absorbed O-H stretching vibration of water molecules belong to the brucite layer at 3445–3500 cm^{-1} [31]. The infrared peaks at 1380 cm^{-1} belong to the C-O vibrational peak (Fig. S2) [32]. In Fig. S2, the absorption peak at 3445–3500 cm^{-1} becomes broad and sharp, indicating that water and interlayer O-H have been removed from the calcined LDH. The C-O vibrational peak at 1380 cm^{-1} disappeared, indicating that carbonate between the layers was removed, which was helpful for the removal of pollution.

3.2. Sorption of humic acids by different LDH

With increasing time, the sorption amount of humic acid by I-LDH and I-CLDH had both increased (Fig. 5). Almost all humic acid was removed by I-CLDH within 200 min, while I-LDH adsorbed only half that amount at this moment. When the time reached 20 h, 4.09 mg/L humic acid was still in the solution. This suggested that the sorption performance of I-CLDH was significantly stronger than that of I-LDH. In addition, the released amount and variation trend of Mg^{2+} and Al^{3+} differed between I-LDH and I-CLDH (Fig. S3). These results are similar to our previously report [18]. During the sorption process, the highest volumes of Mg^{2+} and Al^{3+} released from I-CLDH were 0.95 mmol/L and 0.44 mol/L, respectively. This concentration of Al ions exceeded the highest content of aluminum, which was regulated in China's national drinking water sanitary standard (GB5749-2006).

Due to the strong interaction between the CO_3^{2-} and the metal layer of LDH, the sorption of other anions

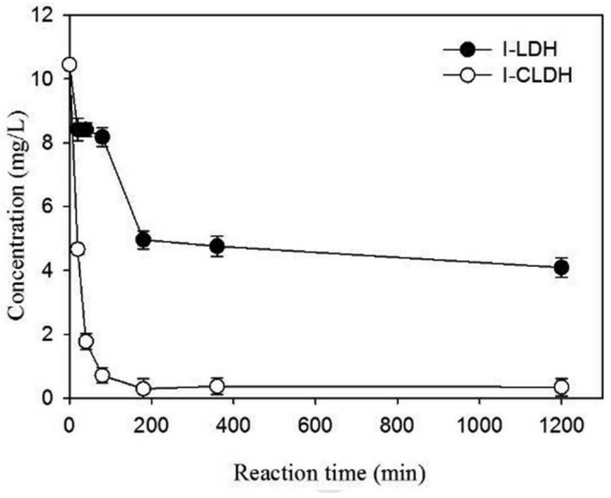

Fig. 5. Changes of humic acid concentrations, Amount of sorbent: 2.5 g/L; initial humic acid concentration: 10.5 mg/L; initial pH: 7.0.

should be hindered by the CO_3^{2-} in the interlayer. However, I-LDH can absorb a certain amount of humic acid. This may be because its particle size is smaller, and most interlayer CO_3^{2-} was at the edge of the laminate and the interaction force between it and the metal laminate was relatively weak [19,24]. Consequently, it was easily exchanged. A further reason may be the high surface area of I-LDH, where part of the humic acid was adsorbed on the surface of metal layer. To illustrate the sorption mechanism of I-CLDH and I-LDH, solid residuals after sorption have been corrected and characterized via FTIR, XRD, and SEM.

Fig. 6 shows an SEM image of I-LDH and I-CLDH after sorption. The morphology of I-LDH after sorbing a certain amount of humic acid showed no noticeable change. In contrast, the structure of I-CLDH also changed from a structure that shows particle accumulation to reticular agglomerates composed by sheet structure. Fig. 7 shows the results of FTIR before and after sorption. No apparent change was found in I-LDH and the remarkable peak at 1360 cm^{-1} still existed, which could be attributed to the anti-symmetric stretching mode of νs (C-O) in CO_3^{2-}. However, for I-CLDH, stretching vibration modes of –CH occurred at 2924 cm^{-1} and 2854 cm^{-1} [33], indicating that humic acid was in the product since the higher sorption capacity of I-CLDH.

In Fig. 8a, the crystal structure of I-LDH remained almost unchanged, but the d-space of I-LDH had increased to 7.54 Å at 3 h and 20 h. This may suggest that ion-exchange between the humic acid and CO_3^{2-} happened in the I-LDH. In contrast to I-LDH, the structure of I-CLDH was gradually transformed from a MgO-like structure to a lamellar crystal structure (Fig. 8b). At 3 h, several characteristic peaks appeared that could be assigned to hydrotalcite. When the time increased to 20 h, the relative intensity increased compared to that at 3 h. Furthermore, similar to I-LDH, the d-spacing of new forming LDH structure from I-CLDH was also 7.54 Å, which suggested that humic acid entered into the interlayer of new forming LDH. However, considering that part of humic acid may have larger length, it would be difficult to enter into the layered structure. Therefore, fractional humic acid may be immobilized on the surface of the metal layer. Fig. 9 summarizes the HA sorption mechanisms on I-LDH and I-CLDH.

3.3. Sorption kinetics and isotherm

Kinetic sorption experiments provide information on the equilibrium time, the sorption rate, and additional parameters that describe the sorption process [34]. Therefore, the sorption data were modeled via pseudo-first [Eq. (1)] and pseudo-second order kinetics [Eq. (2), Fig. S4] [35]:

$$\ln(Q_e - Q_t) = \ln Q_e - k_1 t \quad (1)$$

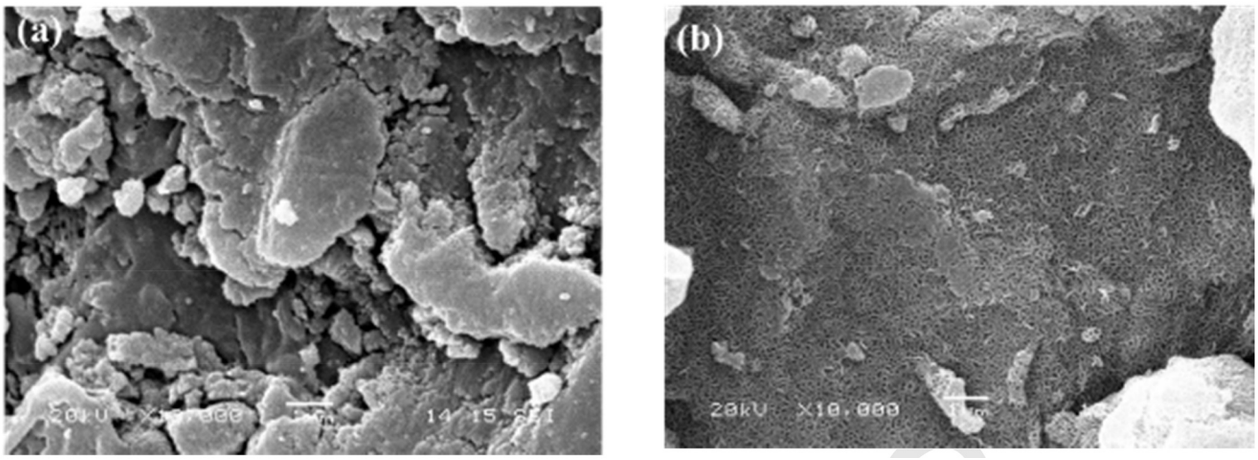

Fig. 6. SEM images of solid residuals after sorption of humic acid (a) I-LDH; (b) I-CLDH.

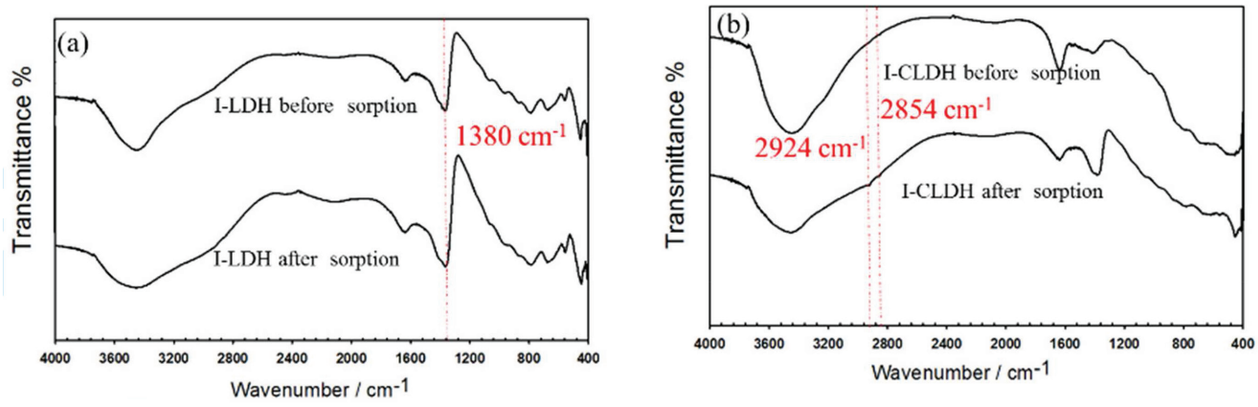

Fig. 7. FTIR spectrum of I-LDH and I-CLDH after sorption.

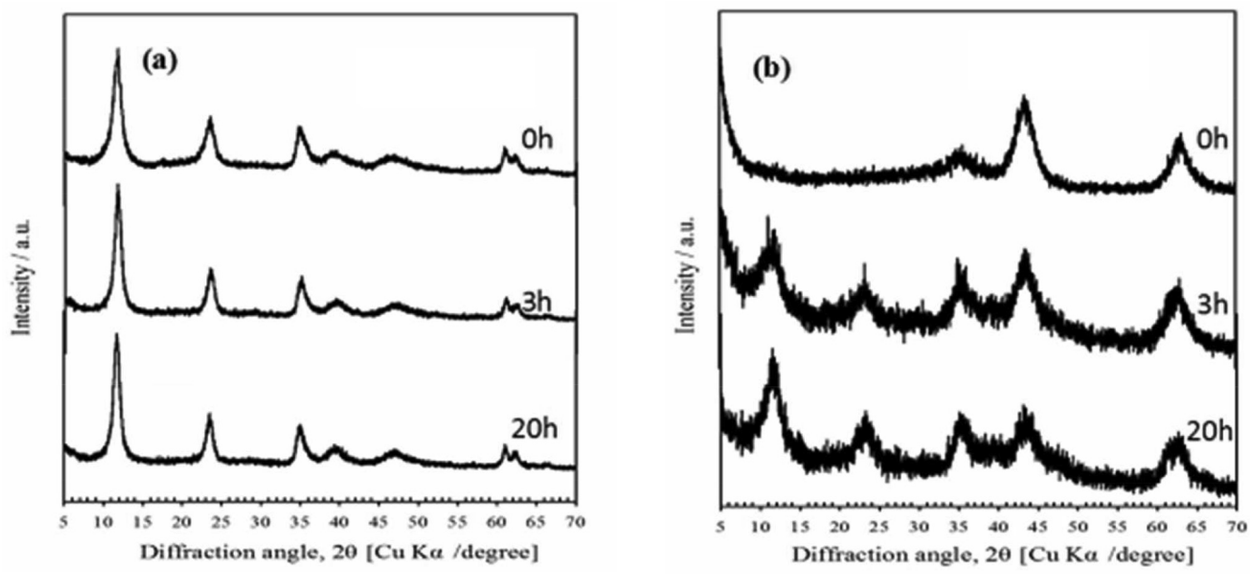

Fig. 8. XRD patterns of (a) I-LDH and (b) I-CLDH after sorption.

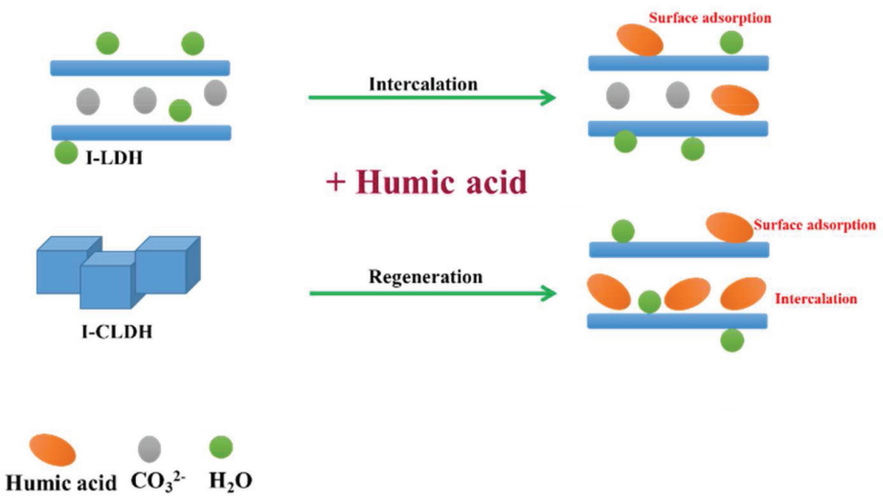

Fig. 9. Schematic diagram of sorption of humic acid via (a) I-LDH and (b) I-CLDH.

$$\frac{t}{Q_e} = \frac{1}{k_2 Q_e^2} + \frac{t}{Q_e} \quad (2)$$

where Q_e (mg/g) and Q_t (mg/g) represent humic acid sorbed at time t and equilibrium time, k_1 (/min) and k_2 represent the sorption rate constant of pseudo first-order kinetic model and pseudo second-order kinetic model, respectively. The calculated kinetic parameter for humic acid removal via I-LDH and I-CLDH are summarized in Table 1. Of the two tested equations, the experimental data showed that both were described slightly better by the pseudo-first order kinetic model based on the correlation coefficient (R^2). Furthermore, for the sorption

Table 1
Sorption kinetic parameters for humic acid sorption onto I-LDH and I-CLDH

Different LDHs	Pseudo first-order kinetic model			Pseudo second-order kinetic model		
	Q_e (mg/g)	k_1 (g/min)	R^2	Q_e (mg/g)	k_2 (g/mg·min)	R^2
I-LDH	2.49	0.0089	0.94	2.82	0.0032	0.93
I-CLDH	3.98	0.0464	0.99	4.17	0.0206	0.97

rate constant (k_2), the highest value was found in I-CLDH, suggesting that sorption equilibrium of I-CLDH could be reached faster than I-LDH. Fig. S5 shows isothermal sorption. According to the experimental data, both Freundlich equation [Eq. (3)] and Langmuir equation [Eq. (4)] were respectively used to fit the sorption isothermal equation [36]:

$$Q_e = K_F \times C_e^{\frac{1}{n}} \tag{3}$$

$$Q\mathrm{e} = \frac{Q_{\max} K_L C_e}{1 + KC_e} \tag{4}$$

where Q_e represents the amount sorbed at equilibrium in mg/g and C_e represents the humic acid concentration at equilibrium, and Q_{max} represents the sorption capacity (mg/g). K_L represents the sorption equilibrium constant (L/mg) and K_F and n represent Freundlich constants, which are related to the sorption capacity and the intensity of sorption, respectively. The calculated parameters and the correlation coefficients (R^2) of both models are provided in Table 2. The highest values of R^2 were obtained with the Langmuir model, which means that this process is a monolayer sorption process. By comparing the Q_{max}, the maximum sorption capacity of I-CLDH was 43.11 mg/g, which was about five times that of I-LDH (8.17 mg/g).

3.4. Effect of Anions on CLDH sorption

Fig. 10 shows that CO_3^{2-}, Cl–, and NO_3^- posed a certain degree of inhibition on the CLDH sorption effect, which was similar to previous reports. Without any other anions, the sorption capacity of I-CLDH was 3.80 mg/g. In the presence of CO_3^{2-}, Cl–, and NO_3, the sorption capacity decreased to 1.34 mg/g, 2.12 mg/g, and 2.47 mg/g, respectively. The average electrostatic potential distribution (ESP) determined via ORCA 3.03 [37] and Multiwfn 3.3 [38] was on the entire molecular surface, and the values of CO_3^{2-}, Cl–, and NO^{3-} were −245.67 kcal/mol, −146.07 kcal/mol, and −128.75 kcal/mol. Since the metal layer was positive, anions with a small electrostatic potential more easily occupied the sorption site of LDH. Therefore, CO_3^{2-} had the smallest electrostatic potential, but its inhibition was the largest in different anions. Although Cl^- and NO_3^- are monovalent anions, the ESP of Cl^- was smaller than that of NO_3^-. Therefore, the inhibitory effect of NO_3^- was lower than that of Cl^-.

Table 2
Sorption isotherm parameters for humic acid sorption via I-LDH and I-CLDH

Different LDHs	Langmuir isotherm model			Freundlich isotherm model		
	Q_{max} (mg/g)	K_L (L/mg)	R^2	K_F (mg$^{1-1/n}$.L$^{1/n}$/g)	1/n	R^2
I-LDH	8.17	0.06	0.92	1.45	0.31	0.83
I-CLDH	43.11	0.35	0.91	16.29	0.19	0.70

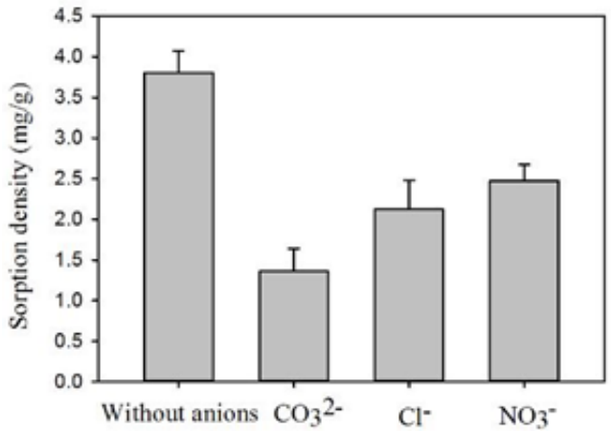

Fig. 10. Effect of coexisting anions on sorption of humic acid onto I-CLDH (sorbents: 2.5 g/L, coexisting anionic concentration: 50 mM; initial humic acid concentration: 10.5 mg/L, initial pH was adjusted to 7.00, reaction time: 20 h).

3.5. Effect of pH on CLDH sorption

The removal of humic acid by I-CLDH was examined at a pH range of 5–11. The amount of humic acid uptake is presented in Fig. 11. When the pH was at around 8, the sorption capacity was 3.81 mg/g. Decreasing the initial pH value to 5 resulted in a sorption capacity of 2.3 mg/L, which is lower than that at pH 8. This was because the acid condition may partially dissolve I-CLDH. In addition, when the initial pH increased to 9 and 11, the sorption capacity decreased to 1.67 and 0.28 mg/g. This suggests that when the pH is too high, hydroxide may compete with humic acid sorption, thus hindering the sorption of humic acid. Another reason is that the surface of LDH is negatively charged in higher pH since the deprotonate happened [2,39]. Humic acid contains carboxylic and phenolic groups and it is negatively charged,

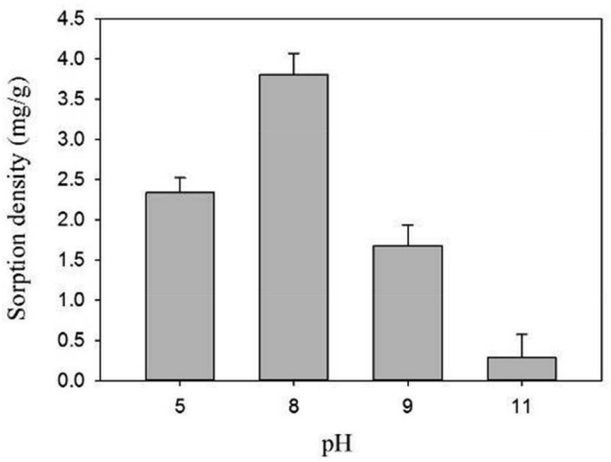

Fig. 11. Effect of pH on sorption of humic acid onto I-CLDH (sorbents: 2.5 g/L, initial humic acid concentration: 10.5 mg/L, initial pH was adjusted to 7.00, reaction time: 20 h).

especially under higher pH conditions [40]. The negatively charged humic acid will be difficult to adsorb on new formation of I-LDH due to electrostatic repulsion, leading to a decrease in sorption at higher pH values (>9).

4. Conclusion

In this study, ultrathin sheets of LDHs with small particle size that were prepared via the ionothermal method in a deep eutectic solvent have been used for the removal of humic acid. By comparing the sorption performance and although CO_3^{2-} species in the I-LDH could be exchanged, samples after calcination showed superior sorption performance. According to the results of XRD, SEM, and FTIR, the sorption process of humic acid via I-CLDH and I-LDH has been suggested. Both the surface reaction and intercalation play an important role in humic acid removal. Since the regeneration happened, I-CLDH could provide more sorption sites for humic acid immobilization and the sorption capacity has been increased. In addition, the high or low pH values in the solution and the common anions in the environment could inhibit the sorption performance of I-CLDH.

Acknowledgment

The study was support by National Natural Science Foundation of China (No. 51504170 and 21571146) and Nature Science Foundation of Hubei Province of China (2015CFB506).

References

[1] W.-W. Tang, G.-M. Zeng, J.-L. Gong, J. Liang, P. Xu, C. Zhang, B.-B. Huang, Impact of humic/fulvic acid on the removal of heavy metals from aqueous solutions using nanomaterials: a review, Sci. Total Environ., 468 (2014) 1014–1027.
[2] G. Zhang, T. Wu, Y. Li, X. Huang, Y. Wang, G. Wang, Sorption of humic acid to organo layered double hydroxides in aqueous solution, Chem. Eng. J., 191 (2012) 306–313.
[3] M. Gasser, H. Mohsen, H. Aly, Humic acid adsorption onto Mg/Fe layered double hydroxide, Colloids Surf. A: Physicochem. Eng. Asp., 331 (2008) 195–201.
[4] S. Vreysen, A. Maes, Adsorption mechanism of humic and fulvic acid onto Mg/Al layered double hydroxides, Appl. Clay Sci., 38 (2008) 237–249.
[5] T. Anirudhan, P. Suchithra, S. Rijith, Amine–modified polyacrylamide–bentonite composite for the adsorption of humic acid in aqueous solutions, Colloids Surf. A: Physicochem. Eng. Asp., 326 (2008) 147–156.
[6] H. Li, Y. Jin, Y. Nie, Application of alkaline treatment for sludge decrement and humic acid recovery, Bioresour. Technol., 100 (2009) 6278–6283.
[7] B.K. Singh, A. Jain, S. Kumar, B.S. Tomar, R. Tomar, V.K. Manchanda, S. Ramanathan, Role of magnetite and humic acid in radionuclide migration in the environment, J. Contam. Hydrol., 106 (2009) 144–149.
[8] B.K. Singh, R. Tomar, S. Kumar, A. Jain, B.S. Tomar, V.K. Manchanda, Sorption of 137Cs, 133Ba and 154Eu by synthesized sodium aluminosilicate (Na-AS), J. Hazard. Mater., 178 (2010) 771–776.
[9] B.K. Singh, J. Bhadauria, R. Tomar, B.S. Tomar, Effect of humic acid on sorption of trace metal ions by sodium aluminosilicate, Desalination, 268 (2011) 189–194.
[10] B.K. Singh, R. Tomar, S. Kumar, A.S. Kar, B.S. Tomar, S. Ramanathan, V.K. Manchanda, Role of the humic acid for sorption of radionuclides by synthesized titania, in: Radiochim. Acta, 2014, pp. 255.
[11] B.K. Singh, F. Mercier-Bion, G. Lefevre, E. Simoni, Effect of short chain aliphatic carboxylic acids for sorption of uranyl on rutile Zeta potential and in situ ATR-FTIR studies, J. Ind. Eng. Chem., 35 (2016) 325–331.
[12] M. Ishaq, S. Sultan, I. Ahmad, H. Ullah, M. Yaseen, A. Amir, Adsorptive desulfurization of model oil using untreated, acid activated and magnetite nanoparticle loaded bentonite as adsorbent, J. Saudi Chem. Soc., 21 (2017) 143–151.
[13] R. Bai, X. Zhang, Polypyrrole-coated granules for humic acid removal, J. Colloid Interface Sci., 243 (2001) 52–60.
[14] R.-X. Wang, T. Wen, X.-L. Wu, A.-W. Xu, Highly efficient removal of humic acid from aqueous solutions by Mg/Al layered double hydroxides–Fe_3O_4 nanocomposites, RSC Adv., 4 (2014) 21802–21809.
[15] Q .Yu, K. Sasaki, K. Tanaka, T. Ohnuki, T. Hirajima, Structural factors of biogenic birnessite produced by fungus Paraconiothyrium sp. WL-2 strain affecting sorption of Co^{2+}, Chem. Geology, 310-311 (2012), 106–113.
[16] A. Jebali, A. Behzadi, I. Rezapor, T. Jasemizad, S. Hekmatimoghaddam, G.H. Halvani, N. Sedighi, Adsorption of humic acid by amine-modified nanocellulose: an experimental and simulation study, Int. J. Environ. Sci. Technol., 12 (2015) 45–52.
[17] K.-H. Goh, T.-T. Lim, Z. Dong, Application of layered double hydroxides for removal of oxyanions: a review, Water Res., 42 (2008) 1343–1368.
[18] X. Qiu, K. Sasaki, T. Hirajima, K. Ideta, J. Miyawaki, Temperature effect on the sorption of borate by a layered double hydroxide prepared using dolomite as a magnesium source, Chem. Eng. J., 225 (2013) 664–672.
[19] Z. Gao, S. Xie, B. Zhang, X. Qiu, F. Chen, Ultrathin Mg-Al layered double hydroxide prepared by ionothermal synthesis in a deep eutectic solvent for highly effective boron removal, Chem. Eng. J., 319 (2017) 108–118.
[20] X. Duan, D.G. Evans, Layered double hydroxides, Springer Science & Business Media, 2006.
[21] L. Fang, W. Li, H. Chen, F. Xiao, L. Huang, P.E. Holm, H.C.B. Hansen, D. Wang, Synergistic effect of humic and fulvic acids on Ni removal by the calcined Mg/Al layered double hydroxide, RSC Adv., 5 (2015) 18866–18874.
[22] F.R. Peligro, I. Pavlovic, R. Rojas, C. Barriga, Removal of heavy metals from simulated wastewater by in situ formation of layered double hydroxides, Chem. Eng. J., 306 (2016) 1035–1040.
[23] L. Ma, Q. Wang, S.M. Islam, Y. Liu, S. Ma, M.G. Kanatzidis, Highly selective and efficient removal of heavy metals by layered double hydroxide intercalated with the $MoS_4^{(2-)}$ ion, J. Am. Chem. Soc., 138 (2016) 2858–2866.
[24] Y. Kuroda, Y. Miyamoto, M. Hibino, K. Yamaguchi, N. Mizuno, Tripodal ligand-stabilized layered double hydroxide nanoparticles with highly exchangeable CO_3^{2-}, Chem. Mater, 25 (2013) 2291–2296.
[25] L. Fang, L. Huang, P.E. Holm, X. Yang, H.C.B. Hansen, D. Wang, Facile upscaled synthesis of layered iron oxide nanosheets and their application in phosphate removal, J. Mater. Chem. A, 3 (2015) 7505–7512.
[26] A. Taubert, Inorganic materials synthesis-a bright future for ionic liquids?, Acta Chim. Slov., 52 (2005) 183.
[27] E.R. Parnham, R.E. Morris, Ionothermal synthesis of zeolites, metal–organic frameworks, and inorganic–organic hybrids, Accounts Chem. Res., 40 (2007) 1005–1013.
[28] D. Freudenmann, S. Wolf, M. Wolff, C. Feldmann, Ionic liquids: new perspectives for inorganic synthesis?, Angewandte Chemie Int. Ed., 50 (2011) 11050–11060.
[29] F. Cavani, F. Trifirò, A. Vaccari, Hydrotalcite-type anionic clays: Preparation, properties and applications, Catal. Today, 11 (1991) 173–301.
[30] F. Millange, R.I. Walton, D. O'Hare, Time-resolved in situ X-ray diffraction study of the liquid-phase reconstruction of Mg–Al–carbonate hydrotalcite-like compounds, J. Mater. Chem., 10 (2000) 1713–1720.

[31] X. Qiu, K. Sasaki, T. Hirajima, K. Ideta, J. Miyawaki, One-step synthesis of layered double hydroxide-intercalated gluconate for removal of borate, Sep. Purif. Technol., 123 (2014) 114–123.
[32] N. Iyi, T. Matsumoto, Y. Kaneko, K. Kitamura, Deintercalation of carbonate ions from a hydrotalcite-like compound: Enhanced decarbonation using acid–salt mixed solution, Chem. Mater., 16 (2004) 2926–2932.
[33] P. Lubal, D. Fetsch, D. Široký, M. Lubalova, J. Šenkýr, J. Havel, Potentiometric and spectroscopic study of uranyl complexation with humic acids, Talanta, 51 (2000) 977–991.
[34] B. Hudcová, V. Veselská, J. Filip, S. Číhalová, M. Komárek, Sorption mechanisms of arsenate on Mg-Fe layered double hydroxides: A combination of adsorption modeling and solid state analysis, Chemosphere, 168 (2017) 539–548.
[35] Y. Guo, Z. Zhu, Y. Qiu, J. Zhao, Adsorption of arsenate on Cu/Mg/Fe/La layered double hydroxide from aqueous solutions, J. Hazard. Mater., 239 (2012) 279–288.
[36] J. Hong, Z. Zhu, H. Lu, Y. Qiu, Synthesis and arsenic adsorption performances of ferric-based layered double hydroxide with α-alanine intercalation, Chem. Eng. J., 252 (2014) 267–274.
[37] F. Neese, The ORCA program system, Wiley Interdisciplinary Reviews: Computational Molecular Science, 2 (2012) 73–78.
[38] T. Lu, F. Chen, Multiwfn: a multifunctional wavefunction analyzer, J. Comput. Chem., 33 (2012) 580–592.
[39] Q. Wang, Y. Gao, J. Luo, Z. Zhong, A. Borgna, Z. Guo, D. O'Hare, Synthesis of nano-sized spherical Mg 3 Al–CO_3 layered double hydroxide as a high-temperature CO_2 adsorbent, RSC Adv., 3 (2013) 3414–3420.
[40] T. Hartono, S. Wang, Q. Ma, Z. Zhu, Layer structured graphite oxide as a novel adsorbent for humic acid removal from aqueous solution, J. Colloid Interface Sci., 333 (2009) 114–119.

Supporting information

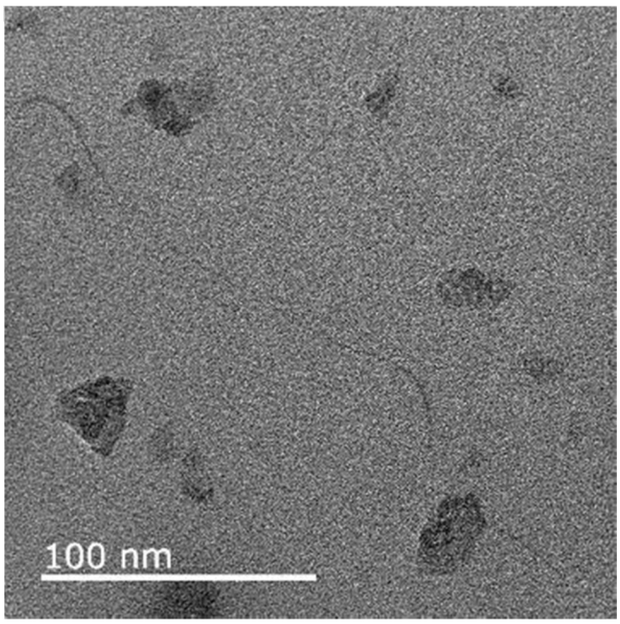

Fig. S1. TEM image of I-CLDH.

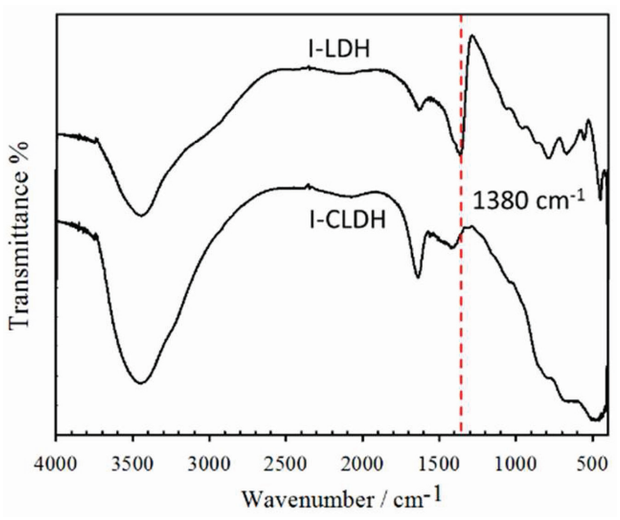

Fig. S2. FTIR spectrum of I-LDH and I-CLDH.

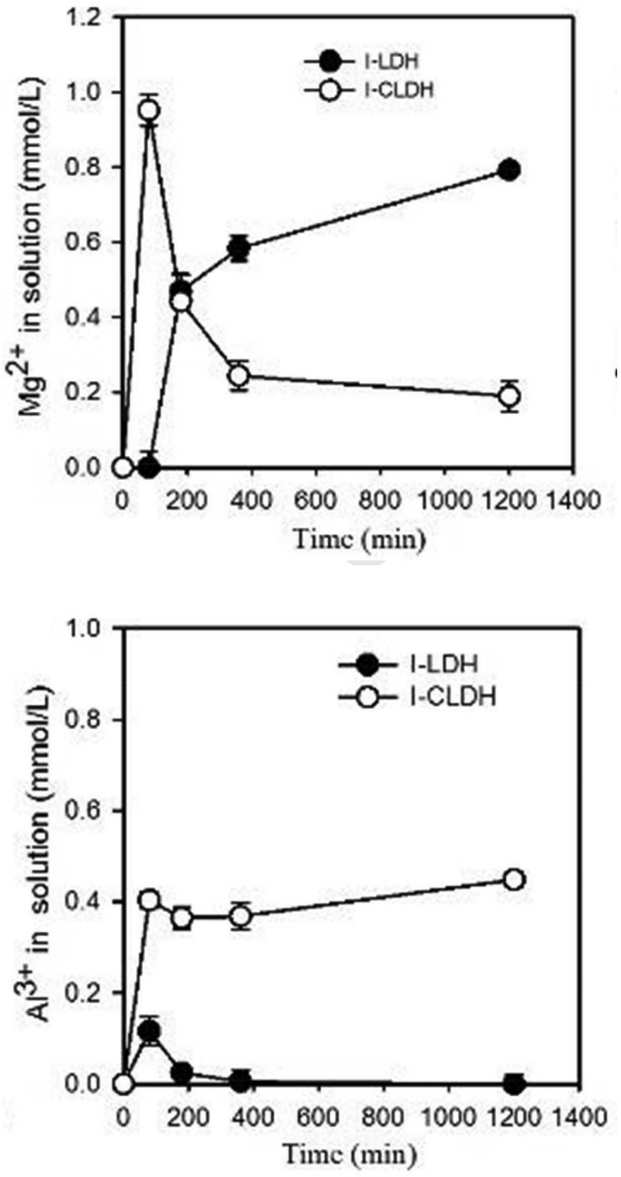

Fig. S3. Fig. 4 Changes of Mg concentration and Al concentration. Amount of sorbent: 2.5 g/L; initial humic acid concentration: 10.5 mg/L; initial pH: 7.0.

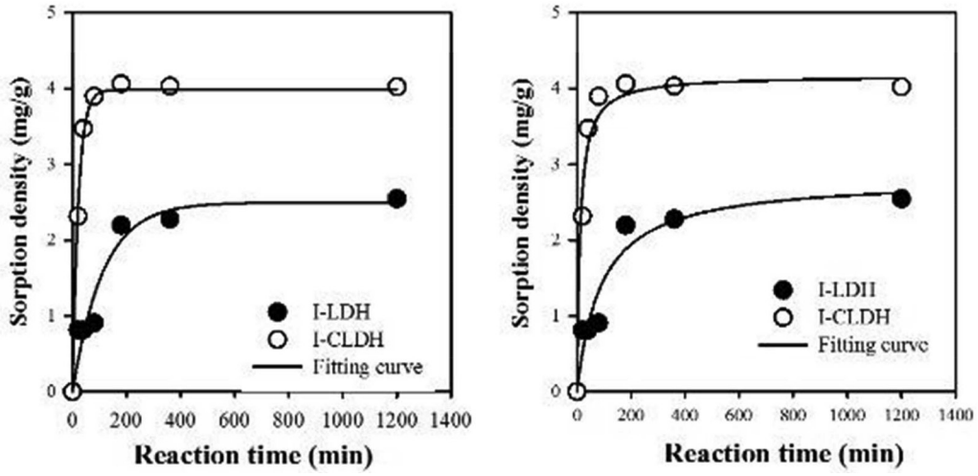

Fig. S4. Sorption kinetics of humic acid via I-LDH and I-CLDH (data used for curve fitting was an average value of three repetitions).

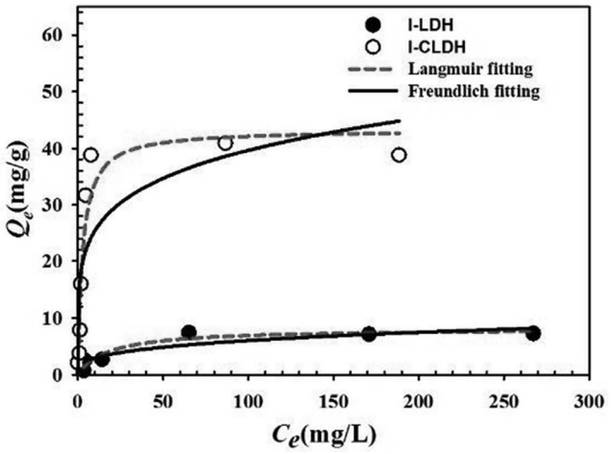

Fig. S5. Sorption isotherms of humic acid via I-LDH and I-CLDH (data used for curve fitting was an average value of three repetitions).